

Efficient prediction of terahertz quantum cascade laser dynamics from steady-state simulations

AGNEW, G., GRIER, A., TAIMRE, T., LIM, Y. L., NIKOLIĆ, M., VALAVANIS, A., COOPER, J., DEAN, P., KHANNA, S. P., LACHAB, M., LINFIELD, E. H., DAVIES, A. G., HARRISON, Paul <<http://orcid.org/0000-0001-6117-0896>>, IKONIĆ, Z., INDJIN, D. and RAKIĆ, A. D.

Available from Sheffield Hallam University Research Archive (SHURA) at:

<https://shura.shu.ac.uk/11143/>

This document is the Published Version [VoR]

Citation:

AGNEW, G., GRIER, A., TAIMRE, T., LIM, Y. L., NIKOLIĆ, M., VALAVANIS, A., COOPER, J., DEAN, P., KHANNA, S. P., LACHAB, M., LINFIELD, E. H., DAVIES, A. G., HARRISON, Paul, IKONIĆ, Z., INDJIN, D. and RAKIĆ, A. D. (2015). Efficient prediction of terahertz quantum cascade laser dynamics from steady-state simulations. *Applied Physics Letters*, 106 (16), p. 161105. [Article]

Copyright and re-use policy

See <http://shura.shu.ac.uk/information.html>

Efficient prediction of terahertz quantum cascade laser dynamics from steady-state simulations

G. Agnew, A. Grier, T. Taimre, Y. L. Lim, M. Nikolić, A. Valavanis, J. Cooper, P. Dean, S. P. Khanna, M. Lachab, E. H. Linfield, A. G. Davies, P. Harrison, Z. Ikonić, D. Indjin, and A. D. Rakić

Citation: *Applied Physics Letters* **106**, 161105 (2015); doi: 10.1063/1.4918993

View online: <http://dx.doi.org/10.1063/1.4918993>

View Table of Contents: <http://scitation.aip.org/content/aip/journal/apl/106/16?ver=pdfcov>

Published by the AIP Publishing

Articles you may be interested in

[Thermo-optic detection of terahertz radiation from a quantum cascade laser](#)

Appl. Phys. Lett. **97**, 251103 (2010); 10.1063/1.3528456

[Nonequilibrium many body theory for quantum transport in terahertz quantum cascade lasers](#)

Appl. Phys. Lett. **95**, 231111 (2009); 10.1063/1.3272675

[The importance of electron temperature in silicon-based terahertz quantum cascade lasers](#)

Appl. Phys. Lett. **95**, 131103 (2009); 10.1063/1.3237177

[Simulated \[111\] Si-SiGe terahertz quantum cascade laser](#)

Appl. Phys. Lett. **92**, 021124 (2008); 10.1063/1.2836023

[13 GHz direct modulation of terahertz quantum cascade lasers](#)

Appl. Phys. Lett. **91**, 143510 (2007); 10.1063/1.2790827

The advertisement for MMR Technologies features a blue and white background with a grid pattern. On the left is the MMR Technologies logo, which consists of the letters 'MMR' in a bold, sans-serif font, with 'TECHNOLOGIES' in a smaller font below it. To the right of the logo is the text 'THE WORLD'S RESOURCE FOR VARIABLE TEMPERATURE SOLID STATE CHARACTERIZATION' in a bold, sans-serif font. Below this text are five images of different types of equipment: 'OPTICAL STUDIES SYSTEMS' (a small, rectangular device), 'SEEBECK STUDIES SYSTEMS' (a blue, rectangular device with a control panel), 'MICROPROBE STATIONS' (a circular, multi-ported device), 'HALL EFFECT STUDY SYSTEMS AND MAGNETS' (a blue, rectangular device with a control panel), and a large, complex magnetic assembly. At the bottom left is the website address 'WWW.MMR-TECH.COM'.

Efficient prediction of terahertz quantum cascade laser dynamics from steady-state simulations

G. Agnew,¹ A. Grier,² T. Taimre,³ Y. L. Lim,¹ M. Nikolić,¹ A. Valavanis,² J. Cooper,² P. Dean,² S. P. Khanna,² M. Lachab,² E. H. Linfield,² A. G. Davies,² P. Harrison,⁴ Z. Ikonić,² D. Indjin,² and A. D. Rakić^{1,a)}

¹*School of Information Technology and Electrical Engineering, The University of Queensland, Brisbane, Queensland 4072, Australia*

²*School of Electronic and Electrical Engineering, University of Leeds, Leeds LS2 9JT, United Kingdom*

³*School of Mathematics and Physics, The University of Queensland, Brisbane, Queensland 4072, Australia*

⁴*Materials and Engineering Research Institute, Sheffield Hallam University, Sheffield S1 1WB, United Kingdom*

(Received 1 March 2015; accepted 13 April 2015; published online 22 April 2015)

Terahertz-frequency quantum cascade lasers (THz QCLs) based on bound-to-continuum active regions are difficult to model owing to their large number of quantum states. We present a computationally efficient reduced rate equation (RE) model that reproduces the experimentally observed variation of THz power with respect to drive current and heat-sink temperature. We also present dynamic (time-domain) simulations under a range of drive currents and predict an increase in modulation bandwidth as the current approaches the peak of the light-current curve, as observed experimentally in mid-infrared QCLs. We account for temperature and bias dependence of the carrier lifetimes, gain, and injection efficiency, calculated from a full rate equation model. The temperature dependence of the simulated threshold current, emitted power, and cut-off current are thus all reproduced accurately with only one fitting parameter, the interface roughness, in the full REs. We propose that the model could therefore be used for rapid dynamical simulation of QCL designs. © 2015 AIP Publishing LLC. [<http://dx.doi.org/10.1063/1.4918993>]

Terahertz-frequency quantum cascade lasers (THz QCLs) are compact, electrically driven sources of coherent radiation in the 1–5 THz band,¹ with peak (pulsed) emission powers now in excess of 1 W and operating temperatures up to 200 K.^{2,3} THz QCLs are also promising continuous-wave (cw) sources, although they have poorer thermal performance and, to date, the maximum achievable cw operating temperature has been ~129 K.⁴ Their carrier dynamics are sensitive to temperature, and the corresponding output power degrades rapidly as temperature increases. As such, there is a requirement to understand and mitigate the influence of the temperature dependence of carrier dynamics upon the QCL behavior. Additionally, the time-domain behavior of modulated THz QCLs is of interest. Due to the absence of relaxation oscillations, the high speed dynamic performance of THz QCLs may be superior to that of diode lasers, potentially making them attractive for high bandwidth communications.^{5,6} The modulation bandwidth of mid-infrared (mid-IR) QCLs varies significantly with respect to the bias current,⁷ but this effect has not been fully investigated in THz QCLs.

Bound-to-continuum (BTC) QCL designs are relatively complex to model, owing to the large number of quantum-confined subbands involved in the active region. Full rate equation (RE) models (i.e., in which all states are considered) yield detailed information about the intersubband transitions, with the dependencies of scattering processes upon temperature and bias being obtained. These models are, however, computationally demanding and are either restricted to

steady-state solutions or relatively simple QCL designs. Furthermore, it is challenging to solve full RE models self-consistently with optical or thermal models. An alternative approach uses a reduced RE (RRE) model, in which a subset of laser parameters is considered: typically, populations of the upper and lower laser levels (ULL/LLL) and the photon density in the cavity. This is advantageous in terms of computational speed, and hence the ability to predict both static *and* dynamic behavior⁸ and to compute the emitted THz power self-consistently. However, the commonly used RRE models^{8–10} treat the laser parameters (carrier lifetimes, gain, and injection efficiencies) as constants, irrespective of bias or lattice temperature. As such, these models are only valid near to the temperature and bias for which the parameters were determined. Moreover, conventional RRE models do not implicitly account for self-heating in the active region, which can be in the tens of Kelvin.¹¹ Although this can be easily dealt with in static simulations, it is problematical where the effect of temperature on the dynamic behavior of the device needs to be considered—it is vital to correctly predict dynamic behavior in, for example, low duty cycle pulsed operation, where the laser is in thermal transient throughout the period for which it is turned on. In this work, we introduce a model that overcomes these difficulties by using a full RE scattering model to obtain the complete temperature and bias (T , V) dependence of the carrier lifetimes, injection efficiencies, and gain. We then use polynomial regressions to these parameters as inputs to a RRE model, which includes the lattice temperature self-consistently through a thermal model of the laser. This gives our model the ability to function correctly over the full operating range

^{a)}Electronic mail: rakic@itee.uq.edu.au

of bias and temperature. Our simulation results reproduce the experimentally observed variations in threshold current, THz power, and cut-off currents and predict a current-dependent variation in modulation bandwidth, which accords with the general expectation that modulation bandwidth increases with internal photon density.¹² Our method is a three-stage process: (1) the Schrödinger and Poisson equations are solved self-consistently with a full RE model of the system that includes all relevant scattering mechanisms¹³ and this is used to deduce the RRE parameters, i.e., ULL and LLL lifetimes, scattering rates between them, injection efficiencies, and gain factor at a range of temperatures and biases; (2) a polynomial function of T and V is fitted to each parameter, thereby producing closed form expressions for inclusion in a RRE model; and (3) the RRE model is solved to obtain carrier and photon populations, using current and ambient (cold finger) temperature as inputs. Stages (1) and (2) are one-off processes that yield a model for a given device and its physical structure. Stage (3) provides the model that can then be executed rapidly for a range of thermal and electrical stimuli being investigated. Our complete model comprising three RREs and a thermal equation reads

$$\frac{dS(t)}{dt} = -\frac{1}{\tau_p} S(t) + M \frac{\beta_{sp}}{\tau_{sp}(T, V)} N_3(t) + MG(T, V)(N_3(t) - N_2(t)) S(t), \quad (1)$$

$$\frac{dN_3(t)}{dt} = -G(T, V)(N_3(t) - N_2(t)) S(t) - \frac{1}{\tau_3(T, V)} N_3(t) + \frac{\eta_3(T, V)}{q} I(t), \quad (2)$$

$$\frac{dN_2(t)}{dt} = +G(T, V)(N_3(t) - N_2(t)) S(t) + \left(\frac{1}{\tau_{32}(T, V)} + \frac{1}{\tau_{sp}(T, V)} \right) N_3(t) - \frac{1}{\tau_{21}(T, V)} N_2(t) + \frac{\eta_2(T, V)}{q} I(t), \quad (3)$$

$$\frac{dT(t)}{dt} = \frac{1}{mc_p} \left(I(t)V(T(t), I(t)) - \frac{(T(t) - T_0(t))}{R_{th}} \right). \quad (4)$$

In Eqs. (1)–(3), $S(t)$, $N_3(t)$, and $N_2(t)$ represent the photon number and the carrier numbers in the ULL and LLL, respectively. The symbol q represents the electronic charge, $I(t)$ is the drive current, V is the voltage across the device terminals, and T is the lattice temperature. Although T and V are themselves time-dependent, this explicit dependence has been suppressed in Eqs. (1)–(3) for readability. The efficiency of carrier injection into the ULL and LLL is given by the terms η_3 and η_2 , respectively. The photon lifetime $\tau_p = 9.015$ ps is calculated from a modal loss of 12.2 cm^{-1} , τ_3 is the total carrier lifetime for non-radiative transitions out of the ULL, τ_{32} is the lifetime for non-radiative transitions from the ULL to the LLL, and τ_{21} is the lifetime for transitions from the LLL to the miniband states. The gain factor as defined in Ref. 8 is represented by G , and $M = 90$ is the total number of periods in the active region structure. The spontaneous emission factor is $\beta_{sp} = 1.627 \times 10^{-4}$ and the spontaneous emission lifetime τ_{sp} is calculated from the relation⁹ $\tau_{sp} = \varepsilon_0 \hbar^3 / 8\pi^2 q^2 n_{\text{eff}}^2 z_{32}^2$ with

the voltage and temperature dependence of z_{32} , the dipole matrix element, accounted for. The symbol $\lambda = 116 \mu\text{m}$ is the emission wavelength and $n_{\text{eff}} = 3.30$ is the effective index of refraction of the optical medium. Equation (4) is the thermal model for the laser, which determines lattice temperature $T(t)$ from the ambient (cold finger) temperature $T_0(t)$ and self-heating caused by excitation current $I(t)$. The thermal resistance between the chip and the cold finger of the cryostat¹⁴ is represented by $R_{th} = 8.2 \text{ KW}^{-1}$, the mass of the chip by $m = 1.533 \times 10^{-8} \text{ kg}$, and the effective specific heat capacity of the chip by $c_p = 330 \text{ J kg}^{-1} \text{ K}^{-1}$. Based on these data, the thermal time constant of the chip, $\tau_T = mc_p R_{th}$, is $41.5 \mu\text{s}$. This figure frames the timescale for which the laser's dynamics is affected by any thermal transient. As the solution of the differential equations progresses, the calculated temperature $T(t)$ is input into Eqs. (1)–(3), thereby continually updating the temperature and voltage-dependent RRE parameters. Therefore, all four equations are coupled and need to be solved simultaneously. Our model does not include the effects of intermodule transit time as discussed in Ref. 8.

The exemplar device selected for simulation is a $11.57 \mu\text{m}$ -thick GaAs/AlGaAs BTC THz QCL with active region structure as described in Ref. 15. The device was processed into a $140 \mu\text{m} \times 1.78 \text{ mm}$ semi-insulating plasmon ridge, and the single-mode emission frequency, measured at threshold, is 2.59 THz . The (T, V) -dependent laser parameters were determined using our full RE model in a grid of 13 temperatures and 38 electric field values, giving a total of 494 grid point values for each parameter. Finally, a smooth function of two variables, lattice temperature T and voltage V , is fitted to the data set for each of the six RRE input parameters using a weighted least squares procedure. From experimental measurements of the device's terminal voltage V at different currents I and cold finger temperatures T_0 , a fitted polynomial model for $V(T(t), I(t))$ is derived in the same way as for the RRE parameters. This model is then used during simulation to determine $V(T(t), I(t))$ in (4). We chose to use experimental I - V characteristics to obtain an accurate measurement of the influence of the impedance of the device contacts and that of our experimental apparatus. An objective of this work was to employ the simplest possible function that allows the RREs to capture the major morphological features of the light-current (L - I) curves. To this end we chose a third order polynomial, which is simple to fit and computationally efficient, making acquisition of data from a large number of simulations practicable in a reasonable time. Derivation of the device-specific model is complete at this point and, together with the RREs and thermal equation, is ready for use.

The ordinary differential equations (1)–(4) may be solved after the current drive function $I(t)$ and cold finger temperature $T_0(t)$ have been defined and initial values for the carrier and photon numbers assumed. The arbitrary but relatively low initial value of 1×10^3 was chosen for $S(t)$, $N_3(t)$, and $N_2(t)$. The optical output power P can then be calculated from the photon number by the relation¹⁶ $P(t) = \eta_0 \hbar \omega S(t) / \tau_p$, where ω is the laser's angular frequency of emission, and $\eta_0 = 0.2593$ is the power output coupling coefficient.¹⁶ In order to simulate the L - I characteristic of the laser, we solved Eqs. (1)–(4) for the case where $I(t)$ is a slow, 1 s duration current sweep from 0.3 to 0.7 A and the cold finger temperature $T_0(t)$ is held

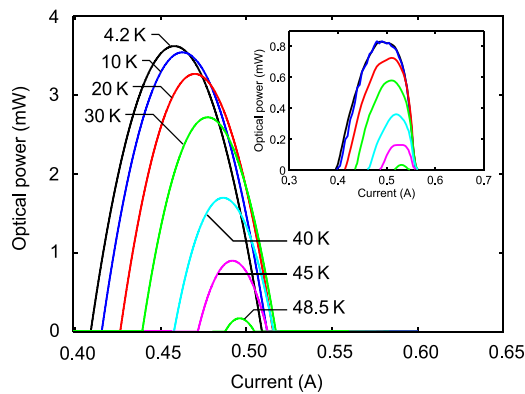


FIG. 1. RRE simulated L - I characteristics of the QCL at seven cold finger temperatures. The curves were generated with a 1 s linear current sweep from 0.3 to 0.7 A while holding $T_0(t)$ constant for each cold finger temperature. Inset: measured L - I characteristics at the same temperatures.

constant. This excitation, when applied to the commonly used RRE model (i.e., with constant parameters), produces an L - I characteristic that is simply a straight line ascending from the threshold current (see Ref. 16). Our simulation correctly reproduces the experimentally observed roll-off in THz power at higher currents over the full range of operating temperatures, as shown in Fig. 1. For comparison, laboratory measured L - I curves for the QCL operating in a continuous-flow cryostat at the same cold finger temperatures are shown inset.

The simulated results compare well with the measured data: threshold current increases with increasing temperature, the peak of the L - I curve diminishes with increasing temperature in the same way as the measured characteristics, and beyond 0.5 A the curves for all temperatures fall off due to field-induced misalignment between the injector and ULL subbands,¹⁷ converging at the same point on the current axis. This is given effect in our model by a rapid decline in the bias-dependent injection efficiency $\eta_3(T, V)$ beyond 3.5 V, which is not present in conventional RRE approaches. We confirmed that the sudden cut-off above 0.5 A is indeed due to subband misalignment by removing the voltage-dependence in the rate equations and observing that the resulting thermal-only rollover occurred much later, beyond 1 A. The simulated dynamic current ranges (i.e., the

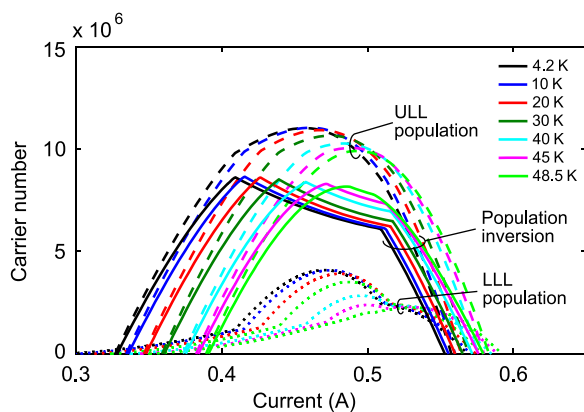


FIG. 2. RRE simulated carrier populations against drive current for seven cold finger temperatures. The curves were generated with a 1 s linear current sweep from 0.3 to 0.6 A while holding $T_0(t)$ constant for each cold finger temperature.

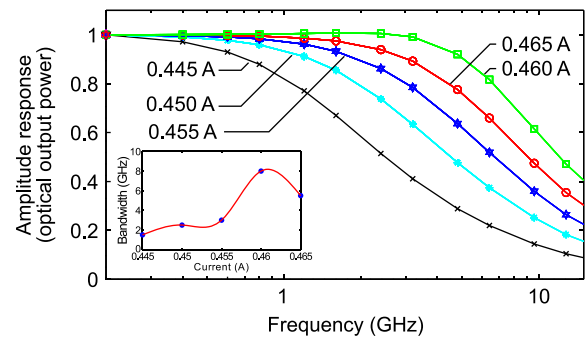


FIG. 3. RRE simulated small signal frequency response at a cold finger temperature of 10 K, for a variety of bias currents. Inset: 3 dB bandwidth for each current—blue dots are data points and the red curve is to guide the eye.

difference between the threshold and cut-off currents) are slightly lower than the experimentally observed value, and the peaks of the L - I curves occur at slightly lower currents. We attribute this to the polynomial fit for η_3 . The substantially lower peak optical power seen in the measurements (0.8 mW as opposed to 3.5 mW in the simulation) is due in part to the poor collection efficiency ($\sim 25\%$) of the detection system used to make the measurement.¹⁸ Figure 2 illustrates the behavior of the population inversion with increasing drive current, at a variety of cold finger temperatures. For reference, the number of carriers in the ULL and LLL are also shown. The simulated small signal frequency response of the device at various bias currents (using a 2 mA peak-to-peak current modulation about the bias point) and a cold finger temperature of 10 K is shown in Fig. 3. From these data, an upper bound for the modulation bandwidth of the laser under various conditions can be determined—for example, to optimize bandwidth for short-range communications.^{5,19} Our model predicts a 3 dB modulation bandwidth between 3 GHz and 10 GHz, with the maximum value being obtained close to the peak of the L - I curve (see inset in Fig. 3). This prediction is the ideal upper bound set by device dynamics and does not include the limitations imposed by external parasitics and possibly the effect of intermodule transit time, which has not been modeled. According to our model, increasing M in Eq. (1) results in increased bandwidth, opposing the effect on bandwidth of intermodule transit

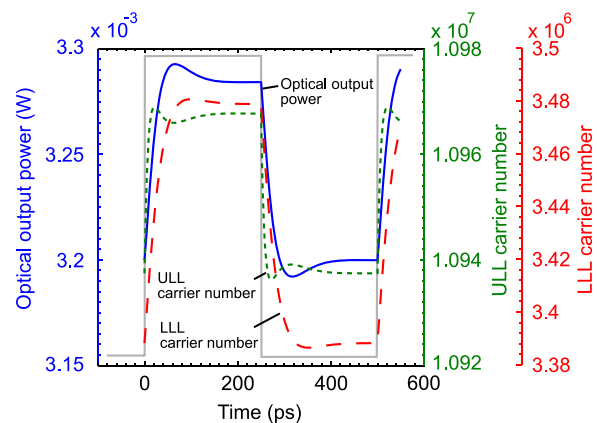


FIG. 4. RRE simulated transient response of the exemplar device to a square wave current stimulus of amplitude 2 mA peak-to-peak. Note that ULL and LLL carrier numbers are effectively clamped. Solid gray line indicates timing of current pulses.

time. To date, there has been limited experimental investigation of the modulation bandwidth of THz QCLs, although device-dependent values of the order of a few GHz have been reported.^{12,19,20} The simulated increase in modulation bandwidth as the drive current approaches the peak of the $L-I$ curve is in qualitative agreement with experimental measurements of mid-IR QCLs,⁷ and this could form the basis of future measurements of THz devices. Time-resolved solutions for the photon and carrier populations in response to high speed square-wave modulation are shown in Fig. 4. The simulation was run at a cold finger temperature of 15 K and a bias current of 0.445 A superimposed on a 2 GHz square wave of amplitude 2 mA peak-to-peak. The response of the photon number in Fig. 4 shows no relaxation oscillation, in accordance with the findings of others.²¹

In summary, we have incorporated the temperature and bias-dependence of the carrier lifetimes, injection efficiencies, and gain in a RRE model of a THz QCL and coupled this with a thermal model. This approach enables the THz power, threshold current, and cut-off current to be determined rapidly over the full range of operating temperatures, with no empirical fitting parameters in the RRE model. We propose that this technique could be used for modeling of THz QCL designs and analysis of their application in high-bandwidth communications and pulsed mode sensing applications.

This research was supported under Australian Research Council's Discovery Projects funding scheme (DP 120 103703). We also acknowledge support of the ERC "NOTES" and "TOSCA" programmes, the EPSRC (UK), the Royal Society, the Wolfson Foundation, and the European Cooperation in Science and Technology (COST) Action BM1205. Y.L.L. acknowledges support under the Queensland Government's Smart Futures Fellowships programme.

- ¹B. S. Williams, *Nature Photon.* **1**, 517 (2007).
- ²L. Li, L. Chen, J. Zhu, J. Freeman, P. Dean, A. Valavanis, A. G. Davies, and E. H. Linfield, *Electron. Lett.* **50**, 309 (2014).
- ³S. Fatholouloumi, E. Dupont, C. Chan, Z. Wasilewski, S. Laframboise, D. Ban, A. Matyas, C. Jirascsek, Q. Hu, and H. C. Liu, *Opt. Express* **20**, 3866 (2012).
- ⁴M. Wienold, B. Röben, L. Schrottke, R. Sharma, A. Tahraoui, K. Biemann, and H. T. Grahn, *Opt. Express* **22**, 3334 (2014).
- ⁵R. Martini and E. A. Whittaker, *J. Opt. Fiber Commun. Rep.* **2**, 279 (2005).
- ⁶Z. Chen, Z. Tan, Y. Han, R. Zhang, X. Guo, H. Li, J. Cao, and H. Liu, *Electron. Lett.* **47**, 1002 (2011).
- ⁷A. Calvar, M. I. Amanti, M. R. St-Jean, S. Barbieri, A. Bismuto, E. Gini, M. Beck, J. Faist, and C. Sirtori, *Appl. Phys. Lett.* **102**, 181114 (2013).
- ⁸Y. Petitjean, F. Destic, J. C. Mollier, and C. Sirtori, *IEEE J. Sel. Top. Quantum Electron.* **17**, 22 (2011).
- ⁹A. Hamadou, S. Lamari, and J. L. Thobel, *J. Appl. Phys.* **105**, 093116 (2009).
- ¹⁰Y. Petitjean, F. Destic, and J. C. Mollier, in *IRMMW-THz Conference Digest of the Joint 32nd International Conference on Infrared and Millimetre Waves and 15th International Conference on Terahertz Electronics* (2007), pp. 476–477.
- ¹¹C. A. Evans, V. D. Jovanović, D. Indjin, Z. Ikonić, and P. Harrison, *IEEE J. Quantum Electron.* **42**, 859 (2006).
- ¹²J. Faist, *Quantum Cascade Lasers* (Oxford University Press, 2013).
- ¹³V. D. Jovanović, S. Höfling, D. Indjin, N. Vukmirović, Z. Ikonić, P. Harrison, J. P. Reithmaier, and A. Forchel, *J. Appl. Phys.* **99**, 103106 (2006).
- ¹⁴M. S. Vitiello, G. Scamarcio, and V. Spagnolo, *Appl. Phys. Lett.* **92**, 101116 (2008).
- ¹⁵A. D. Rakić, T. Taimre, K. Bertling, Y. L. Lim, P. Dean, D. Indjin, Z. Ikonić, P. Harrison, A. Valavanis, S. P. Khanna, M. Lachab, S. J. Wilson, E. H. Linfield, and A. G. Davies, *Opt. Express* **21**, 22194 (2013).
- ¹⁶A. Hamadou, J. L. Thobel, and S. Lamari, *Opt. Commun.* **281**, 5385 (2008).
- ¹⁷S. S. Howard, Z. Liu, and C. F. Gmachl, *IEEE J. Quantum Electron.* **44**, 319 (2008).
- ¹⁸A. Tredicucci, R. Köhler, L. Mahler, H. E. Beere, E. H. Linfield, and D. A. Ritchie, *Semicond. Sci. Technol.* **20**, S222 (2005).
- ¹⁹S. Barbieri, W. Maineult, S. S. Dhillon, C. Sirtori, J. Alton, N. Breuil, H. E. Beere, and D. A. Ritchie, *Appl. Phys. Lett.* **91**, 143510 (2007).
- ²⁰W. Maineult, L. Ding, P. Gellie, P. Filloux, C. Sirtori, S. Barbieri, T. Akalin, J.-F. Lampin, I. Sagnes, H. E. Beere, and D. A. Ritchie, *Appl. Phys. Lett.* **96**, 021108 (2010).
- ²¹R. Paiella, R. Martini, F. Capasso, C. Gmachl, H. Y. Hwang, D. L. Sivco, J. N. Baillargeon, A. Y. Cho, E. A. Whittaker, and H. C. Liu, *Appl. Phys. Lett.* **79**, 2526 (2001).